

Evolution of an Accretion Disc in Binary Black Hole Systems

Shigeo S. Kimura^{1,2,3*}, Sanemichi Z. Takahashi², and Kenji Toma^{1,2}

¹Frontier Research Institute for Interdisciplinary Sciences, Tohoku University, Sendai 980-8578, Japan

²Astronomical Institute, Tohoku University, Sendai 980-8578, Japan

³Department of Astronomy & Astrophysics, Pennsylvania State University, University Park, PA 16802, USA

Accepted XXX. Received YYY; in original form ZZZ

ABSTRACT

We investigate evolution of an accretion disc in binary black hole (BBH) systems and possible electromagnetic counterparts of the gravitational waves from mergers of BBHs. Perna et al. (2016) proposed a novel evolutionary scenario of an accretion disc in BBHs in which a disc eventually becomes “dead”, i.e., the magnetorotational instability (MRI) becomes inactive. In their scenario, the dead disc survives until *a few seconds before* the merger event. We improve the dead disc model and propose another scenario, taking account of effects of the tidal torque from the companion and the critical ionization degree for MRI activation more carefully. We find that the mass of the dead disc is much lower than that in the Perna’s scenario. When the binary separation sufficiently becomes small, the mass inflow induced by the tidal torque reactivates MRI, restarting mass accretion onto the black hole. We also find that this disc “revival” happens *thousands of years before* the merger. The mass accretion induced by the tidal torque increases as the separation decreases, and a relativistic jet could be launched before the merger. The emissions from these jets are too faint compared to GRBs, but detectable if the merger events happen within $\lesssim 10$ Mpc or if the masses of the black holes are as massive as $\sim 10^5 M_\odot$.

Key words: accretion, accretion discs — gravitational waves — black hole physics — gamma-ray burst: general — X-rays: binaries

1 INTRODUCTION

The Laser Interferometer Gravitational-wave Observatory (LIGO) detected gravitational wave (GW) signals from merger events of binary black hole (BBH) systems (Abbott et al. 2016a,b). Although electromagnetic counterparts of GWs from mergers of BBHs were unexpected, the *Fermi* Gamma-ray Burst Monitor (GBM) reported detection of gamma-rays from the consistent direction of GW150914 (Connaughton et al. 2016), which indicates possibility of a short gamma-ray burst (GRB) coincident with the merger of BBH¹. While some claim that the GBM event is likely to be a false signal (Lyutikov 2016; Greiner et al. 2016; Xiong 2016), some models are proposed to explain it (Perna et al. 2016; Janiuk et al. 2016; Loeb 2016). Possible electromagnetic counterparts in other wavelengths are also discussed (Murase et al. 2016; Yamazaki et al. 2016). For producing

powerful radiation, it is necessary to leave sufficient amount of material around the merging black holes (BHs). Here, we study disc accretion in BBHs.

The evolution of an accretion disc is determined by the efficiency of angular momentum transport. It is believed that turbulent stress induced by the magnetorotational instability (MRI) can efficiently transport the angular momentum (Balbus & Hawley 1991, 1998). This instability is active for ionized plasma, whereas it is suppressed when the ionization degree is sufficiently low (Gammie 1996; Menou et al. 2001). If the disc is MRI “dead”, the disc material can remain around BHs for a long time. Perna et al. (2016) argued that the dead disc can remain until a few seconds before the merger, and can supply energy enough to explain the GBM event. However, their model seems to ignore or misestimate a few processes that affect evolution of an accretion disc in binary systems. One important process is the effect of tidal torque, which prevents the disc material from expanding outward beyond the tidal truncation radius (Ichikawa & Osaki 1994). This causes the disc to evolve as a different solution from well-known self-similar solutions (e.g.

* E-mail: shigeo@astr.tohoku.ac.jp

¹ No electromagnetic counterparts have been reported for GW151226 (Racusin et al. 2016; Smartt et al. 2016)

Cannizzo et al. 1990; Menou et al. 2001; Perna et al. 2016). Another important point is the critical ionization degree for MRI activation, which depends on physical quantities of the disc. Since MRI is active for very low ionization degree (e.g. Gammie 1996; Sano & Miyama 1999), the critical temperature for MRI activation is lower than that expected in Perna’s scenario where they use the temperature at which disc opacity changes from bound-free and free-free opacity to H^- opacity.

In this paper, we improve the dead disc model and propose another scenario, which predicts electromagnetic counterparts of GWs whose luminosity increases with time. In Figure 1, we show the schematic evolutionary tracks of the disc mass, the mass accretion rate, and the binary separation. The disc experiences three phases. At first, the disc forgets its initial condition through viscous evolution. Then, the disc mass and the accretion rate decrease with radiative cooling, which leads to decrease of the ionization degree (phase I). This eventually suppresses MRI, forming a dead disc that remains around the BH until the binary separation sufficiently decreases (phase II). Then, the heating by the tidal torque from the companion becomes effective, which reactivates MRI in the entire region of the disc, restarting accretion onto the BH (phase III-i). This disc “revival” happens many years before the merger². We describe this model in detail in Section 2. The mass accretion rate increases as the separation decreases, and a relativistic jet could be launched owing to high accretion rate (phase III-ii). We estimate flux of electromagnetic emission from the jet and discuss its detectability in Section 3. Section 4 is devoted to summary and discussion.

2 EVOLUTION OF A DISC IN BBH SYSTEMS

2.1 Initial evolution

We consider an equal-mass binary of initial separation R_{ini} and mass of BHs M_{BH} , where the separation should be small such that the binary can merge in the Hubble time. Some mechanisms are proposed to realize this situation, such as the common envelope evolution (Kinugawa et al. 2014; Belczynski et al. 2016) and/or the friction by dense gas (Bartos et al. 2016). We focus on an accretion disc around one of the BHs. We do not discuss the origin of this disc, which might be fallback material of supernova explosion (e.g., Perna et al. 2014) or a tidally disrupted object (e.g., Seto & Muto 2011).

Consider a gas ring around a BH. The ring expands both inward and outward due to the viscous diffusion to become an accretion disc (e.g., Pringle 1981). When the outer radius of the disc, r_{out} , becomes close to R_{ini} , the tidal torque from the companion prevents the disc from expanding outward (Papaloizou & Pringle 1977; Artymowicz & Lubow 1994; Ichikawa & Osaki 1994). The balance between the viscous torque and tidal torque determines the disc radius, and it is expected that the outer radius of the disc is fixed at

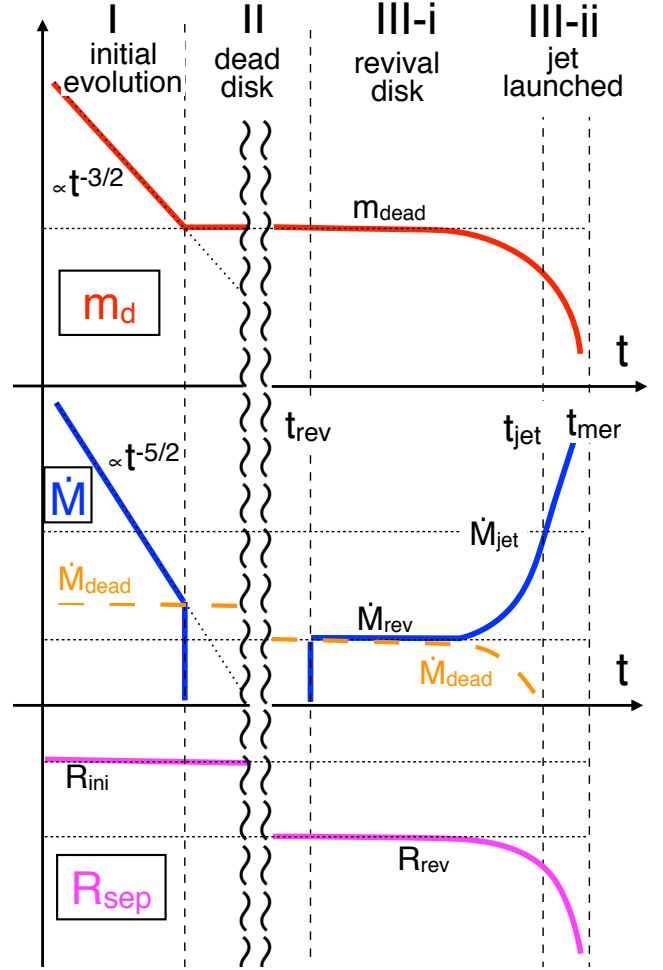


Figure 1. Schematic evolutionary tracks of the disc mass (red), the mass accretion rate (blue), and the binary separation (magenta). Note that this is double logarithmic plot and that phase II is much longer than the other phases.

$r_{\text{out}} \sim a_{\text{sep}} R_{\text{ini}}$, where we introduce a separation parameter a_{sep} . We fix $a_{\text{sep}} = 0.3$ in this paper for simplicity (Paczynski 1977). The disc expands to r_{out} in the viscous time (e.g. Pringle 1981)

$$t_{\text{vis}} = \frac{1}{\alpha \Omega_K} \left(\frac{r_{\text{out}}}{H} \right)^2 \sim 2.6 \times 10^4 a_{-0.5}^{3/2} R_{12}^{3/2} M_{1.5}^{-1/2} \alpha_{-1}^{-1} \left(\frac{r_{\text{out}}}{H} \right)^2 \text{ s}, \quad (1)$$

where $\Omega_K = \sqrt{GM_{\text{BH}}/r^3}$ is the Keplerian angular velocity, $H = c_s/\Omega_K$ is the scale height (c_s is the sound speed), $r_{\text{out}} \simeq a_{\text{sep}} R_{\text{ini}}$, $M_{1.5} = M_{\text{BH}}/30 M_\odot$, $\alpha_{-1} = \alpha/0.1$, $R_{12} = R_{\text{ini}}/(10^{12} \text{ cm})$, and $a_{-0.5} = a_{\text{sep}}/0.3$. We use the alpha prescription for viscosity, $\nu = \alpha c_s^2/\Omega_K$. On the other hand, the time scale of GW inspiral is (e.g. Shapiro & Teukolsky 1983)

$$t_{\text{mer}} = \frac{5}{512} \frac{c^5}{G^3} \frac{R_{\text{ini}}^4}{M_{\text{BH}}^3} \sim 3.8 \times 10^{15} R_{12}^4 M_{1.5}^{-3} \text{ s}. \quad (2)$$

We can see $t_{\text{vis}} < t_{\text{mer}}$ for $r_{\text{out}}/H \lesssim 10^5$, which is valid in all the situations we usually expect. Thus, the disc forgets its initial mass and/or radius due to viscous evolution before the merger.

² Perna et al. (2016) mentioned a low-luminosity and long-lasting transient preceding the merger by the MRI reactivation due to photons from the outer rim, although they did not discuss it in detail.

For the well-known solution of an accretion disc around single BHs, the disc outer radius increases with time as a result of the outward angular momentum transport (Lynden-Bell & Pringle 1974). On the other hand, in a binary system, the angular momentum of the disc material is carried to the companion by the tidal torque. Therefore, the disc material can accrete onto the BH without increasing the disc outer radius. Note that the tidal heating and torque are effective only in very thin outer rim located just outside r_{out} (Ichikawa & Osaki 1994). Almost all the mass is in the viscously heated region of $r \leq r_{\text{out}}$, and the mass that expands beyond r_{out} is expected to be negligible. Note that the merging time t_{mer} is unchanged by the angular momentum transport from the disc to the companion if the mass of the disc is much lower than that of the companion.

We consider evolution of the disc in a binary system, assuming opacity of the disc is constant, $\kappa = 0.4 \text{ cm}^2 \text{ g}^{-1}$, for simplicity. The viscous heating and radiative cooling rates are

$$Q_{\text{vis}} = \frac{9}{8} \nu \Sigma \Omega_K^2, \quad (3)$$

$$Q_{\text{rad}} = \frac{8\sigma_{\text{sb}} T^4}{3\kappa \Sigma}, \quad (4)$$

respectively. The thermal balance, $Q_{\text{vis}} = Q_{\text{rad}}$, gives the disc temperature as

$$T = \left(\frac{27k_B \kappa}{64\sigma_{\text{sb}} m_p} \right)^{1/3} \alpha^{1/3} \Omega_K^{1/3} \Sigma^{2/3}, \quad (5)$$

where we use $c_s^2 = k_B T / m_p$. The viscous time is shorter in the inner region of the disc, where the steady state is realized (e.g., Lynden-Bell & Pringle 1974). The mass accretion rate onto the BH is estimated to be

$$\dot{M} = 3\pi \nu \Sigma \propto \Sigma^{5/3} \Omega_K^{-2/3}. \quad (6)$$

Since this mass accretion rate is constant for the inner region, the radial profile of the surface density is $\Sigma \propto r^{-3/5}$. Using this profile, we estimate the disc mass to be

$$m_d = \int_{r_{\text{in}}}^{r_{\text{out}}} 2\pi \Sigma r dr \approx \frac{10\pi}{7} \Sigma_{\text{out}} r_{\text{out}}^2, \quad (7)$$

where $\Sigma_{\text{out}} = \Sigma(r = r_{\text{out}})$. Note that treatment of r_{out} (fixed as $a_{\text{sep}} R_{\text{sep}}$) is crucial for tracking the evolution of m_d because it strongly depends on r_{out} .

Ignoring wind mass loss, the disc mass decreases according to Equation (6). Then, we can write the evolution of disc mass as

$$\frac{dm_d}{dt} = -\dot{M} = f(R_{\text{ini}}, a_{\text{sep}}, M_{\text{BH}}, \alpha) m_d^{5/3}, \quad (8)$$

where we set $R_{\text{sep}} \approx R_{\text{ini}}$, since $t_{\text{vis}} \ll t_{\text{mer}}$. Then, we can integrate this equation and obtain

$$m_d = m_{d,\text{ini}} \left(\frac{t}{t_{\text{ini}}} \right)^{-3/2}, \quad (9)$$

where $m_{d,\text{ini}}$ is the disc mass at the time $t = t_{\text{ini}}$.

To confirm this scaling relation, we numerically solve the diffusion equation of viscous disc evolution:

$$\frac{\partial \Sigma}{\partial t} = \frac{1}{r} \frac{\partial}{\partial r} \left[\frac{1}{dj/dr} \frac{\partial}{\partial r} \left(\nu \Sigma r^3 \frac{d\Omega}{dr} \right) \right], \quad (10)$$

with a boundary condition $\dot{M} = 0$ at $r = r_{\text{out}}$. This treatment corresponds to the assumption (introduced above) that

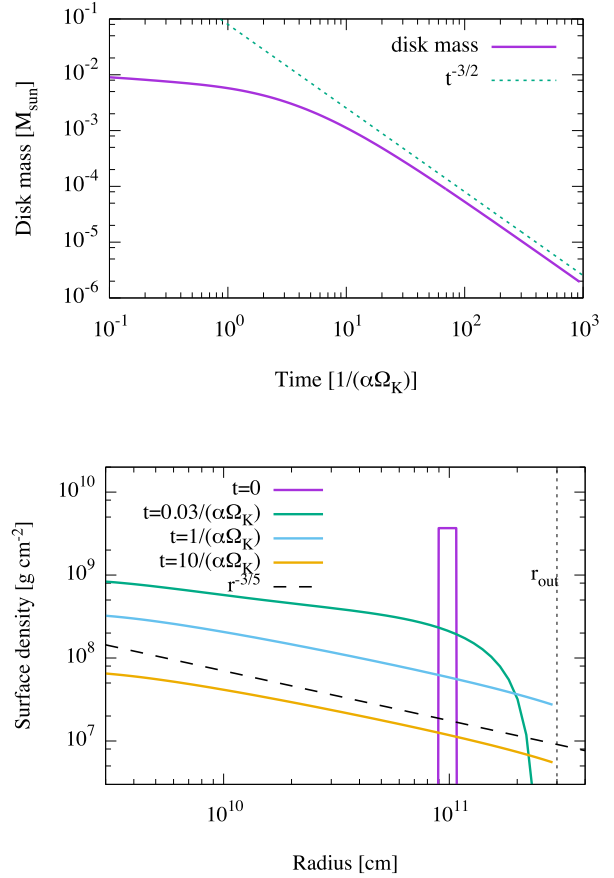


Figure 2. The results of the numerical calculation of the diffusion equation. The upper panel shows the evolution of disc mass. The numerical calculation (solid line) matches the analytic model (dotted line) for $t \gtrsim 5/(\alpha \Omega_K)$. The lower panel shows the radial profile of the surface density. The vertical dotted line shows the outer boundary. The profiles are single power-law for $t \gtrsim 1/(\alpha \Omega_K)$, and the material does not accumulate near r_{out} .

the tidal torque is effective only in the very thin outer rim just outside $r = r_{\text{out}}$ (Ichikawa & Osaki 1994). That is, the disc evolution at $r < r_{\text{out}}$ is governed by the viscous torque as described by Equation (10), and the tidal torque is balanced to the viscous torque just at $r = r_{\text{out}}$. The disc material at $r = r_{\text{out}}$, receives the angular momentum from the material at $r < r_{\text{out}}$ by the viscous torque. The same amount of angular momentum is transported to the companion by the tidal torque, which makes the angular momentum flux constant at $r = r_{\text{out}}$. Therefore, the disc material at $r = r_{\text{out}}$ does not expand further. We initially put a gas ring of $m_{d,\text{ini}} = 0.01 M_{\odot}$ at $r = 10^{11} \text{ cm}$. We use the reference parameter set ($\alpha = 0.1$, $M_{\text{BH}} = 30 M_{\odot}$, $R_{\text{ini}} = 10^{12} \text{ cm}$, and $a_{\text{sep}} = 0.3$). We show the results of the numerical calculation in Figure 2. The upper panel shows the evolution of disc mass, which matches our analytic model in later time. The lower panel shows the radial profiles of the surface density at $t = 0$, $t = 0.03/(\alpha \Omega_K)$, $t = 1/(\alpha \Omega_K)$, and $t = 10/(\alpha \Omega_K)$, where we use Ω_K at $r = r_{\text{out}}$. The disc material expands both inward and outward, and reaches the outer boundary at $t \sim 1/(\alpha \Omega_K)$. After that, its profile is expressed as a single power-law of $r^{-3/5}$. This means that the disc material

does not accumulate near $r = r_{\text{out}}$, implying that the mass may be estimated by Equation (7).

If MRI is always active, this scaling relation is applicable all the time. Setting $t_{\text{ini}} = t_{\text{vis}}$, we estimate the disc mass at the time of merger and find that it is 10^{-11} times lower than the initial disc mass, where we use the reference parameter set used in Equation (1) and $(r_{\text{out}}/H) \sim 100$. Even if $m_{\text{d,ini}}$ is as massive as $100M_{\odot}$, the disc mass of the merging time is $10^{-9} M_{\odot}$. This is too low to produce energetic electromagnetic counterparts of GW signals, which requires $m_{\text{d}} \sim 10^{-5} M_{\odot}$ (Murase et al. 2016; Lyutikov 2016).

2.2 Formation of a dead disc

The disc cools down as the disc becomes lighter, which changes the disc state from fully-ionized plasma to almost neutral. The MRI is inactive if the ionization degree sufficiently decreases. The condition for MRI to be active is (e.g., Sano & Miyama 1999; Okuzumi & Hirose 2011; Fujii et al. 2014)

$$\Lambda = \frac{v_A^2}{\eta \Omega_K} > 1, \quad (11)$$

where Λ is the Elsasser number, v_A is the Alfvén velocity, and η is the resistivity. The resistivity in accretion discs, where the Ohmic dissipation is dominant, is $\eta = 234(T/1\text{K})^{1/2} \chi_e^{-1} \text{cm}^2 \text{s}^{-1}$ (Blaes & Balbus 1994). Writing $v_A^2 = 2c_s^2/\beta_{\text{pl}}$, the instability condition is

$$\chi_e > \chi_{\text{dead}} = \frac{117T^{1/2}\beta_{\text{pl}}\Omega_K}{c_s^2} \simeq 9.9 \times 10^{-10} \beta_2 T_{3.5}^{-1/2} M_{1.5}^{1/2} a_{-0.5}^{-3/2} R_{12}^{-3/2}, \quad (12)$$

where $\chi_e = n_e/n$ is the ionization degree ($n = \Sigma/(2m_p H)$ is the total number density), $\beta_{\text{pl}} = 8\pi P/B^2$ is the plasma beta (P is the gas pressure), $T_{3.5} = T/(3000 \text{ K})$, and $\beta_2 = \beta_{\text{pl}}/(10^2)$. The MRI is active even for such a low ionization degree, which makes the mass of the dead disc lower than that in Perna et al. (2016).

We calculate the ionization degree in the accretion disc by solving the Saha's equation. Since BHs heavier than $\sim 10M_{\odot}$ are expected to form only under low-metallicity environments (Abbott et al. 2016c), we consider pure hydrogen discs. Then, the Saha's equation is

$$\frac{\chi_e^2}{1 - \chi_e} = \frac{1}{n} \left(\frac{2\pi m_e k_B T}{h^2} \right)^{3/2} \exp\left(-\frac{E_i}{k_B T}\right), \quad (13)$$

where $E_i = 13.6 \text{ eV}$. Since the ionization degree exponentially decreases with temperature, the outer edge of the viscously heated region ($r = r_{\text{out}}$) is the first place which becomes dead. When the dead region appears at $r = r_{\text{out}}$, the mass inflow to the inner region ($r < r_{\text{out}}$) stops, which causes the inner region of $r < r_{\text{out}}$ to cool down rapidly due to the lack of heating source. Thus, the dead region propagates inward, and the entire region of the disc becomes dead (formation of a dead disc). Using equation (5), (12), and (13), we calculate the critical temperature T_{dead} below which MRI is dead for given β_{pl} and R_{ini} . We find that $2600 \text{ K} < T_{\text{dead}} < 4000 \text{ K}$ for $10 \leq \beta_{\text{pl}} \leq 10^3$ and $10^{11} \text{ cm} < R_{\text{ini}} < 3 \times 10^{12} \text{ cm}$. The parameter dependence of T_{dead} is so weak that we can hereafter estimate physical quantities by approximating $T_{\text{dead}} \sim 3000 \text{ K}$.

The mass of the dead disc is estimated to be

$$m_{\text{dead}} \approx \frac{80\pi}{21} \left(\frac{\sigma_{\text{sb}} m_p}{3k_B \kappa} \right)^{1/2} \left(\frac{T_{\text{dead}}^3}{\alpha \Omega_K} \right)^{1/2} r_{\text{out}}^2 \quad (14)$$

$$\simeq 1.1 \times 10^{-8} T_{\text{d},3.5}^{3/2} \alpha_{-1}^{-1/2} M_{1.5}^{-1/4} R_{12}^{11/4} a_{0.5}^{11/4} M_{\odot},$$

where $T_{\text{d},3.5} = T_{\text{dead}}/(3000 \text{ K})$ we use Equation (5) and (7). Note that this m_{dead} is independent of the disc initial condition, although the initial mass $m_{\text{d,ini}}$ appears in Equation (9). The initial condition affects the time when the disc becomes dead. We find that for our fiducial parameter set, m_{dead} is lower than the required mass for the luminous electromagnetic counterparts, $\sim 10^{-5} M_{\odot}$ (Murase et al. 2016; Lyutikov 2016). Since m_{dead} strongly depends on R_{ini} , the dead disc for $R_{\text{ini}} \gtrsim 10^{13} \text{ cm}$ can be massive enough to emit luminous electromagnetic counterparts. While t_{mer} is longer than Hubble time for such a wide separation, rapid separation decrease might occur by some mechanisms, such as friction by dense gas (e.g., Bartos et al. 2016). The critical mass accretion rate for MRI activation is

$$\begin{aligned} \dot{M}_{\text{dead}} &= 3\pi\nu\Sigma_{\text{out}} \\ &= 8\pi \left(\frac{k_B \sigma_{\text{sb}}}{3\kappa m_p} \right)^{1/2} \alpha^{1/2} \Omega_K^{-3/2} T_{\text{dead}}^{5/2} \\ &\simeq 3.3 \times 10^{16} \alpha_{-1}^{1/2} M_{1.5}^{-3/4} R_{12}^{9/4} a_{0.5}^{9/4} T_{\text{d},3.5}^{5/2} \text{ g s}^{-1}, \end{aligned} \quad (15)$$

where we use Equations (5) and (6). Once the disc becomes dead, it remains until the binary separation sufficiently decreases. Although we derive Equation (15) at $r = r_{\text{out}}$, this equation is valid for arbitrary radius. Note that \dot{M}_{dead} is an increasing function of the radius r . In this situation, the inner region is always active for MRI whenever the outer region is active as discussed in the next subsection.

2.3 Revival of a dead disc

The binary separation, R_{sep} , decreases owing to emission of gravitational waves even for the dead disc phase (phase II in Figure 1). The decrease of the binary separation causes the decrease of r_{out} , beyond which the tidal torque is effective. Then, the amount of gas in the outer rim ($r > r_{\text{out}}$) increases. The angular momentum of the gas in $r > r_{\text{out}}$ is transported to the companion by the tidal torque. This induces the mass inflow from the outer rim to the dead disc. Therefore, the decrease of the binary separation provides the mass inflow from the outer rim to the dead disc, which can reactivate the MRI.

The decreasing rate of the separation is (e.g. Shapiro & Teukolsky 1983)

$$v_{\text{GW}} = \frac{dR_{\text{sep}}}{dt} = -\frac{128G^3 M_{\text{BH}}^3}{5c^5 R_{\text{sep}}^3}. \quad (16)$$

Assuming $r_{\text{out}} = a_{\text{sep}} R_{\text{sep}}$ with constant a_{sep} , the decreasing rate of the disc outer radius is written as $a_{\text{sep}} v_{\text{GW}}$. We write the surface density of the dead disc as $\tilde{\Sigma} \sim m_{\text{dead}}/(\pi r_{\text{out}}^2)$. Then, the mass inflow rate caused by the separation decrease is estimated to be

$$\dot{M}_{\text{SD}} = -2\pi r_{\text{out}} \tilde{\Sigma} a_{\text{sep}} v_{\text{GW}} \sim -\frac{2m_{\text{dead}} v_{\text{GW}}}{R_{\text{sep}}}. \quad (17)$$

When \dot{M}_{SD} becomes higher than \dot{M}_{dead} at r_{out} , the mass inflow by the tidal torque reactivates MRI at the outermost

region of the dead disc. This is because the mass inflow releases the gravitational energy, causing to heat up gas in the outermost region³. The turbulent stress causes the gas of the outermost active region to fall to the inner dead region of $r < r_{\text{out}}$ with the mass inflow rate \dot{M}_{SD} ⁴, which heats up gas at the inner dead region. This heating rate is high enough to activate MRI in the inner dead region because $\dot{M}_{\text{SD}} > \dot{M}_{\text{dead}}(r_{\text{out}}) > \dot{M}_{\text{dead}}(r)$, and the MRI active region propagates inward with the local viscous time. Therefore, once the mass inflow activates MRI at $r \sim r_{\text{out}}$, the whole part of the disc inevitably becomes active, restarting the mass accretion onto the BH. This disc “revival” happens when $\dot{M}_{\text{SD}} = \dot{M}_{\text{dead}}(r_{\text{out}})$. The separation at that time is

$$R_{\text{rev}} = \left[\frac{32m_{\text{dead}}}{5\pi c^5} \left(\frac{3m_p \kappa}{k_B \sigma_{\text{sb}} \alpha} \right)^{1/2} \frac{(GM_{\text{BH}})^{15/4}}{a_{\text{sep}}^{9/4} T_{\text{dead}}^{5/2}} \right]^{4/25} \quad (18)$$

$$\sim 7.3 \times 10^{10} m_{-8}^{4/25} \alpha_{-1}^{-2/25} a_{0.5}^{-9/25} M_{1.5}^{3/5} T_{d,3.5}^{-2/5} \text{ cm},$$

where $m_{-8} = m_{\text{dead}}/(10^{-8} M_{\odot})$. When the disc revives, $t_{\text{vis}} \sim t_{\text{GW}}$ is satisfied because $\dot{M}_{\text{dead}} \sim m_{\text{dead}}/t_{\text{vis}}$ and $\dot{M}_{\text{SD}} \sim m_{\text{dead}}/t_{\text{GW}}$.

After the revival, the separation decreasing rate is likely to control the mass accretion rate onto the BH as⁵

$$\dot{M}_{\text{GW}} = -2\pi r_{\text{out}} \Sigma_{\text{out}} a_{\text{sep}} v_{\text{GW}} = -\frac{7m_d v_{\text{GW}}}{5R_{\text{sep}}}, \quad (19)$$

where we use the disc profile of the steady disc solution as phase I, $\Sigma \propto r^{-5/3}$ and $\Sigma_{\text{out}} = 7m_d/(10\pi r_{\text{out}}^2)$ (see Subsection 2.1). The disc temperature is determined so that $t_{\text{GW}} \sim t_{\text{vis}}$ at $r = r_{\text{out}}$ is satisfied. Using the relation $dm_d/dt = -\dot{M}_{\text{GW}}$, we can write $dm_d/dR_{\text{sep}} = 7m_d/(5R_{\text{sep}})$, which is integrated as

$$m_d = m_{\text{dead}} \left(\frac{R_{\text{sep}}}{R_{\text{rev}}} \right)^{7/5}. \quad (20)$$

Since the mass of the dead disc is conserved during phase II, $m_d = m_{\text{dead}}$ for $R_{\text{sep}} = R_{\text{rev}}$. Also, we can integrate Equation (16) and obtain

$$R_{\text{sep}} = R_{\text{rev}} \left(\frac{t_{\text{mer}} - t}{t_{\text{mer}} - t_{\text{rev}}} \right)^{1/4}, \quad (21)$$

where t_{rev} is the time when the disc revives. The time from the revival to the merger is very long,

$$t_{\text{mer}} - t_{\text{rev}} = \frac{5}{512} \frac{c^5}{G^3} \frac{R_{\text{rev}}^4}{M_{\text{BH}}^3} \quad (22)$$

$$\sim 1.1 \times 10^{11} m_{-8}^{16/25} \alpha_{-1}^{-8/25} a_{0.5}^{-36/25} M_{1.5}^{-3/5} T_{d,3.5}^{-8/5} \text{ s}.$$

³ The heating rate by mass inflow is $\sim \dot{M} \Omega_K^2$. This determines the temperature at the outermost region of the disc by $\dot{M} \Omega_K^2 \sim Q_{\text{rad}}(T)$. On the other hand, using Equation (3), (4) and (6), Equation (15) is rewritten as $\dot{M}_{\text{dead}} \Omega_K^2 \sim Q_{\text{rad}}(T_{\text{dead}})$. This equation is the same form as that of the mass inflow. Therefore, we can use Equation (15) as the condition for MRI activation because $T > T_{\text{dead}}$ is approximately equivalent to $\dot{M} > \dot{M}_{\text{dead}}$.

⁴ The gas of the MRI active region inevitably falls to the inner region even if the inner region is dead, because the viscous stress transports the angular momentum at the active region (e.g. Zhu et al. 2010; Suzuki et al. 2010).

⁵ Two \dot{M} introduced in this subsection is different: \dot{M}_{SD} is the mass inflow rate from the outer rim to the dead disc and \dot{M}_{GW} is the mass accretion rate from the revival disc to the central BH.

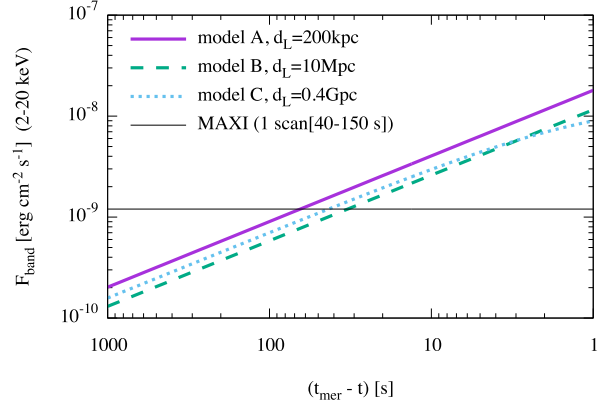


Figure 3. The photon fluxes from the internal shocks for models A, B, and C. The 1-scan sensitivity of MAXI GSC is also plotted. It is found that all the models are detectable by MAXI GSC.

Equation (20) and (21) lead to

$$m_d = m_{\text{dead}} \left(\frac{t_{\text{mer}} - t}{t_{\text{mer}} - t_{\text{rev}}} \right)^{7/20}. \quad (23)$$

The mass accretion rate is

$$\dot{M}_{\text{GW}} = \frac{7m_{\text{dead}}}{20(t_{\text{mer}} - t_{\text{rev}})} \left(\frac{t_{\text{mer}} - t}{t_{\text{mer}} - t_{\text{rev}}} \right)^{-13/20}. \quad (24)$$

For $t < t_{\text{mer}}$, \dot{M}_{GW} is almost constant,

$$\dot{M}_{\text{rev}} \simeq \frac{7m_{\text{dead}}}{20(t_{\text{mer}} - t_{\text{rev}})} \quad (25)$$

$$\sim 6.4 \times 10^{13} m_{-8}^{9/25} \alpha_{-1}^{8/25} a_{0.5}^{36/25} M_{1.5}^{3/5} T_{d,3.5}^{8/5} \text{ g s}^{-1}.$$

This solution indicates that the tidal torque controls the mass accretion rate such that $\dot{M}_{\text{rev}} \sim \dot{M}_{\text{dead}}$, marginally keeping steady accretion, as shown in Figure 1. This accretion rate is so low that it is difficult to observe it. For $t \lesssim t_{\text{mer}}$, the mass accretion rate increases with time as $\propto (t_{\text{mer}} - t)^{-13/20}$. This situation continues until $\alpha^{-1} \Omega_K^{-1} > R_{\text{sep}}/v_{\text{GW}}$ is satisfied, which is just before the merger (0.005 s for $M_{\text{BH}} = 30 M_{\odot}$ and $\alpha = 0.1$). After that, a smooth accretion flow no longer exists, and a shocked-violent accretion is likely to take place (Farris et al. 2015).

3 DETECTABILITY OF ELECTROMAGNETIC COUNTERPARTS

The accretion rate can exceed the Eddington accretion rate (at t_{jet} in Figure 1). A relativistic jet is expected to be launched from the accreting BH in such a situation (Tchekhovskoy et al. 2011). We consider $\dot{M}_{\text{GW}} \sim \dot{M}_{\text{jet}} \equiv 10L_{\text{Edd}}/c^2$ at the jet launching. We estimate the kinetic luminosity of the jet to be $L_{\text{jet}} \sim \dot{M}_{\text{GW}} c^2$. The high-energy photons are produced in internal shocks within the jet, whose bolometric luminosity and flux at the Earth are estimated to be $L_{\gamma} \sim \eta_{\gamma} L_{\text{jet}}$ and $F_{\gamma} = L_{\gamma}/(4\pi d_L^2)$, respectively, where η_{γ} is the radiative efficiency of the internal shocks and d_L is the luminosity distance. The observed time of these photons after the jet launch is $\Delta t_{\gamma} \sim R_s/c \sim 3 \times 10^{-4} M_{1.5}$ s, where R_s is the Schwarzschild radius of the BH, so that these photons arrive at the Earth before the GW signal.

Table 1. Parameters and physical quantities related to the electromagnetic counterparts from jets

model	$M_{\text{BH}} [M_{\odot}]$	$R_{\text{ini}} [\text{cm}]$	$(t_{\text{mer}} - t_{\text{jet}}) [\text{s}]$	$L_{\text{AG}} [\text{erg s}^{-1}]$	$T_{\text{AG}} [\text{s}]$	$d_{\text{L,limit}} [\text{Mpc}]$
A	30	3×10^{12}	5.0×10^3	3.8×10^{40}	3.2×10^2	19
B	10^3	3×10^{13}	4.7×10^4	1.3×10^{42}	2.2×10^3	1.1×10^2
C	10^5	10^{15}	4.4×10^6	1.3×10^{44}	4.5×10^4	1.1×10^3

The jet sweeps up gas surrounding the BBH and creates an external shock, which emits broadband photons, i.e., afterglow. The bolometric luminosity of the afterglow is estimated to be

$$L_{\text{AG}} \sim \frac{E_{\text{jet}}(t)}{t - t_{\text{jet}}} = \frac{\int_{t_{\text{jet}}}^t L_{\text{jet}} dt'}{t - t_{\text{jet}}}, \quad (26)$$

where $E_{\text{jet}}(t)$ is the time integrated energy and t_{jet} is the jet launching time. Since the jet luminosity for $t_{\text{jet}} < t < t_{\text{mer}}$ is almost constant⁶, $E_{\text{jet}}(t)$ is proportional to $(t - t_{\text{jet}})$. Thus, this luminosity is almost constant, $L_{\text{AG}} \sim \dot{M}_{\text{GW}} c^2 \sim 10 L_{\text{Edd}}$ for $t_{\text{jet}} < t < t_{\text{mer}}$. The photons of the afterglow arrive at the Earth both before and after the GW signal. The duration of the bright afterglow phase after the GW signal is

$$T_{\text{AG}} \sim \frac{R_{\text{AG}}}{2c\Gamma_{\text{jet}}^2} = \left(\frac{3E_{\text{jet}}(t = t_{\text{mer}})}{4\pi m_p c^5 n_{\text{ext}} \Gamma_{\text{jet}}^8} \right)^{1/3}, \quad (27)$$

where R_{AG} is the deceleration radius, n_{ext} is the density of the surrounding gas, and Γ_{jet} is the Lorentz factor of the jet.

We discuss detectability of the emission from the jets for three models: model A assumes massive stellar mass BHs that corresponds to the system of GW150914 (Abbott et al. 2016a), model B assumes intermediate mass BHs (IMBH) that are expected to exist in the center of star cluster (e.g., Gerssen et al. 2002), and model C assumes massive BHs (MBH) that may be formed by collapse of supermassive stars (e.g., Shapiro & Teukolsky 1983), for which M_{BH} , R_{ini} , and resultant physical quantities are tabulated in Table 1. The other parameters are fixed as $\alpha = 0.1$, $T_{\text{dead}} = 3000 \text{ K}$, $a_{\text{sep}} = 0.3$, $\Gamma_{\text{jet}} = 10$, and $n_{\text{ext}} = 1 \text{ cm}^{-3}$. The durations of the jet launch and the afterglow are longer for higher M_{BH} and larger R_{ini} , and L_{AG} is proportional to M_{BH} .

Figure 3 shows time evolution of the internal shock emission flux in a certain energy band, $F_{\text{band}} = \eta_{\text{band}} F_{\gamma}$, for models A, B, and C with the values of d_{L} . We set $\eta_{\text{band}} \eta_{\gamma} \sim 0.1$ for simplicity. The 1-scan sensitivity of Gas Slit Camera (GSC) on Monitor of All-sky X-ray Image (MAXI) for an energy range 2 keV–20 keV is also plotted (Negoro et al. 2016). Since it takes 40 s–150 s for the 1-scan of MAXI, these jets are detectable if F_{band} at $t_{\text{mer}} - t = 40 \text{ s}$ is higher than the sensitivity. We can see that the emissions are marginally detectable for all the models. Since the sensitivity of *Swift* Burst Alert Telescope (BAT) for 15 keV–150 keV with exposure time of 40 s is comparable to that of MAXI (Barthelmy et al. 2005), these jets are detectable even if they mainly emit hard X-rays. This emission is a unique electromagnetic counterpart of GWs from merging BBHs in the sense that it can be detectable before the GW

signal and that the luminosity increases with time. However, the luminosity and total energy are too low to explain GRBs or the GBM event (Connaughton et al. 2016).

The optical follow-up surveys for GW counterparts, such as the Pan-STARRS1 and the Japanese collaboration for Gravitational wave ElectroMagnetic follow-up (J-GEM), have a sensitivity of 19–21 magnitude (Smartt et al. 2016; Morokuma et al. 2016). Assuming 10 % of L_{AG} is in the optical range, we calculate the distance of detection limit for the afterglow, $d_{\text{L,lim}}$, whose values are tabulated in Table 1. Owing to the good sensitivity, the optical follow-up surveys of afterglows can detect more distant events than the X-ray monitoring systems. However, $d_{\text{L,lim}}$ for model A is shorter than the distance of the observed GW events (Abbott et al. 2016a,b). Although $d_{\text{L,lim}}$ is larger for IMBHs and MBHs, we do not discuss the detection probability because the merger rates of IMBH binaries and MBH binaries are very uncertain.

4 SUMMARY & DISCUSSION

We study evolution of an accretion disc in BBH systems and propose an evolutionary track of the disc, which leads to different conclusion from the previous work (Perna et al. 2016). At first, the disc viscously expands outward but the companion prevents the disc from expanding beyond r_{out} due to the tidal torque. The evolution of viscous disc results in the decrease of the disc mass and the temperature. When the disc sufficiently cools down (typically less than 3000 K), the dead disc forms because MRI becomes inactive. As the binary separation decreases, the position at which the tidal torque is effective moves inward, and the mass of the outer rim increases. Then, the angular momentum is transported by the tidal torque, which induces the mass inflow from the outer rim to the dead disc. When the mass inflow by the tidal torque becomes higher than \dot{M}_{dead} , the accretion heating activates MRI, restarting the mass accretion from the disc to the central black hole (the disc revival). This disc revival typically happens thousands of years before the merger event. The evolution of the revival disc is determined by the tidal torque, keeping $t_{\text{vis}} \sim t_{\text{GW}}$. The mass accretion rate of the revival disc increases with time.

In the late phase of the revival disc evolution, the mass accretion rate can exceed Eddington rate, and a relativistic jet is expected to be launched. We estimate the electromagnetic flux from the jet and discuss its detectability. Since the jet luminosity is increasing with time, the X-ray flux from the internal shock increases with time. This flux can be detectable before the merger event. The afterglow can typically be luminous a few hundreds seconds after the merger. The estimated flux from the jet is too low to explain the GBM event, but detectable by the optical transient surveys

⁶ For $t_{\text{jet}} < t < t_{\text{mer}}$, \dot{M}_{GW} appears to be rapidly increasing in Figure 1, while we can see $\dot{M}_{\text{GW}} \approx \text{const}$ if we plot \dot{M}_{GW} as a function of $(t - t_{\text{jet}})$.

or X-ray monitoring systems if the merger events happen in the local universe ($\lesssim 10$ Mpc) or if BHs are very massive ($\sim 10^5 M_\odot$).

In Section 2.1, we ignore the slim disc regime (Abramowicz et al. 1988), which is realized when the mass accretion is super Eddington. In this regime, disc mass decreases more rapidly than the standard disc regime we use. The slim disc regime ends when the mass accretion rate becomes lower than the Eddington rate. Since \dot{M}_{dead} is lower than the Eddington rate, the standard disc regime takes place whenever disc becomes dead. Thus, our conclusion does not change even if we properly take the slim disc regime into account, although the timescale when the disc becomes dead is modified.

In Section 2.2, we ignore ionization by cosmic rays (CRs), although its effect for accretion process is still under debate (e.g., Bai & Stone 2013). The CRs ionize the disc surface layer of $\Sigma_z = \int_z^\infty \rho(z) dz \lesssim 100 \text{ g cm}^{-2}$, where $\rho(z)$ is the density (Umebayashi & Nakano 1981). Assuming the density of CRs is the same as that in the interstellar medium of the Galaxy, we write the ionization rate as $\zeta_{\text{cr}} \sim 10^{-17} \text{ cm}^3 \text{ s}^{-1}$ (Umebayashi & Nakano 1981). The equilibrium condition between the ionization by CRs and recombination is $\zeta_{\text{cr}} n_H = \beta_{\text{rec}} n_e n_p$, where $\beta_{\text{rec}} = 6.22 \times 10^{-13} T_{3.5}^{-3/4}$ is the radiative recombination rate (the UMIST database, McElroy et al. 2013). Assuming $n_H = \Sigma/(2m_p H)$, $n_e = n_p$, and $n_e = \chi_e n_H$, we obtain the equilibrium ionization degree χ_{cr} . The instability condition for MRI is $\chi_{\text{dead}} \leq \chi_{\text{cr}}$. We calculate the critical β_{p1} below which the MRI is active, whose values are 26, 2.2×10^2 , and 8.9×10^3 for models A, B, and C in Section 3, respectively. Since the expected value of β_{p1} by the MRI turbulence ranges 10–100, the layered accretion is likely for models B and C. In this case, the surface layer of $\Sigma_{\text{active}} \sim 100 \text{ g cm}^{-2}$ accretes onto BHs (Gammie 1996). The mass loss by the layered accretion in t_{mer} is estimated to be $M_{\text{lay}} \sim 3\pi\nu\Sigma_{\text{active}}t_{\text{mer}}$, the values of which are $46 M_\odot$, $68 M_\odot$, and $1.6 \times 10^3 M_\odot$ for models A, B, and C, respectively. These values are much higher than the mass of the dead disc. Therefore, some mechanism to reduce CR density is necessary to leave the dead disc until the disc revives for models B and C.

In Section 2.3, we use some assumptions such as constant separation parameter ($a_{\text{sep}} = 0.3$) and $\tilde{\Sigma} \sim m_{\text{dead}}/(\pi r_{\text{out}}^2)$. In order to verify these assumptions, we should perform long-term non-ideal magneto-hydrodynamical simulations with cold fluid and non-axisymmetric gravity. This is because (a) the viscous time is much longer than the dynamical time, (b) the resistivity is essential for the death and revival of the disc, (c) the sound speed in the disc is much slower than the Keplerian velocity, and (d) tidal torque is non-axisymmetric effect. Such simulations remain as a future work.

ACKNOWLEDGEMENTS

We thank Takanori Sakamoto, Kohta Murase, and Yuri Fujii for useful comments. This work is partly supported by JST grant “Building of Consortia for the Development of Human Resources in Science and Technology” (S.S.K. and K.T.) and JSPS Grants-in-Aid for Scientific Research 15H05437 (K.T.).

REFERENCES

- Abbott B. P., et al., 2016a, *Physical Review Letters*, **116**, 061102
 Abbott B. P., et al., 2016b, *Physical Review Letters*, **116**, 241103
 Abbott B. P., et al., 2016c, *ApJ*, **818**, L22
 Abramowicz M. A., Czerny B., Lasota J. P., Szuszkiewicz E., 1988, *ApJ*, **332**, 646
 Artymowicz P., Lubow S. H., 1994, *ApJ*, **421**, 651
 Bai X.-N., Stone J. M., 2013, *ApJ*, **769**, 76
 Balbus S. A., Hawley J. F., 1991, *ApJ*, **376**, 214
 Balbus S. A., Hawley J. F., 1998, *Reviews of Modern Physics*, **70**, 1
 Barthelmy S. D., et al., 2005, *Space Sci. Rev.*, **120**, 143
 Bartos I., Kocsis B., Haiman Z., Márka S., 2016, preprint, ([arXiv:1602.03831](https://arxiv.org/abs/1602.03831))
 Belczynski K., Holz D. E., Bulik T., O’Shaughnessy R., 2016, preprint, ([arXiv:1602.04531](https://arxiv.org/abs/1602.04531))
 Blaes O. M., Balbus S. A., 1994, *ApJ*, **421**, 163
 Cannizzo J. K., Lee H. M., Goodman J., 1990, *ApJ*, **351**, 38
 Connaughton V., et al., 2016, preprint, ([arXiv:1602.03920](https://arxiv.org/abs/1602.03920))
 Farris B. D., Duffell P., MacFadyen A. I., Haiman Z., 2015, *MNRAS*, **447**, L80
 Fujii Y. I., Okuzumi S., Tanigawa T., Inutsuka S.-i., 2014, *ApJ*, **785**, 101
 Gammie C. F., 1996, *ApJ*, **457**, 355
 Gerssen J., van der Marel R. P., Gebhardt K., Guhathakurta P., Peterson R. C., Pryor C., 2002, *AJ*, **124**, 3270
 Greiner J., Burgess J. M., Savchenko V., Yu H.-F., 2016, preprint, ([arXiv:1606.00314](https://arxiv.org/abs/1606.00314))
 Ichikawa S., Osaki Y., 1994, *PASJ*, **46**, 621
 Janiuk A., Bejger M., Charzynski S., Sukova P., 2016, preprint, ([arXiv:1604.07132](https://arxiv.org/abs/1604.07132))
 Kinugawa T., Inayoshi K., Hotokezaka K., Nakauchi D., Nakamura T., 2014, *MNRAS*, **442**, 2963
 Loeb A., 2016, *ApJ*, **819**, L21
 Lynden-Bell D., Pringle J. E., 1974, *MNRAS*, **168**, 603
 Lyutikov M., 2016, preprint, ([arXiv:1602.07352](https://arxiv.org/abs/1602.07352))
 McElroy D., Walsh C., Markwick A. J., Cordiner M. A., Smith K., Millar T. J., 2013, *A&A*, **550**, A36
 Menou K., Perna R., Hernquist L., 2001, *ApJ*, **559**, 1032
 Morokuma T., et al., 2016, *PASJ*,
 Murase K., Kashiya K., Mészáros P., Shoemaker I., Senno N., 2016, *ApJ*, **822**, L9
 Negoro H., et al., 2016, *PASJ*, **68**, S1
 Okuzumi S., Hirose S., 2011, *ApJ*, **742**, 65
 Paczynski B., 1977, *ApJ*, **216**, 822
 Papaloizou J., Pringle J. E., 1977, *MNRAS*, **181**, 441
 Perna R., Duffell P., Cantiello M., MacFadyen A. I., 2014, *ApJ*, **781**, 119
 Perna R., Lazzati D., Giacomazzo B., 2016, *ApJ*, **821**, L18
 Pringle J. E., 1981, *ARA&A*, **19**, 137
 Racusin J. L., et al., 2016, preprint, ([arXiv:1606.04901](https://arxiv.org/abs/1606.04901))
 Sano T., Miyama S. M., 1999, *ApJ*, **515**, 776
 Seto N., Muto T., 2011, *MNRAS*, **415**, 3824
 Shapiro S. L., Teukolsky S. A., 1983, Black holes, white dwarfs, and neutron stars: The physics of compact objects
 Smartt S. J., et al., 2016, preprint, ([arXiv:1606.04795](https://arxiv.org/abs/1606.04795))
 Suzuki T. K., Muto T., Inutsuka S.-i., 2010, *ApJ*, **718**, 1289
 Tchekhovskoy A., Narayan R., McKinney J. C., 2011, *MNRAS*, **418**, L79
 Umebayashi T., Nakano T., 1981, *PASJ*, **33**, 617
 Xiong S., 2016, preprint, ([arXiv:1605.05447](https://arxiv.org/abs/1605.05447))
 Yamazaki R., Asano K., Ohira Y., 2016, *Progress of Theoretical and Experimental Physics*, **2016**, 051E01
 Zhu Z., Hartmann L., Gammie C., 2010, *ApJ*, **713**, 1143

This paper has been typeset from a $\text{\TeX}/\text{\LaTeX}$ file prepared by the author.